



Research Article

# Interface-facilitated stable plasticity in ultra-fine layered FeAl/FeAl<sub>2</sub> micro-pillar at high temperature

Lulu Li<sup>a</sup>, Irene J. Beyerlein<sup>b</sup>, Weizhong Han<sup>a,\*</sup>



<sup>a</sup> Center for Advancing Materials Performance from the Nanoscale, State Key Laboratory for Mechanical Behavior of Materials, Xi'an Jiaotong University, Xi'an 710049, China

<sup>b</sup> Department of Mechanical Engineering, Materials Department, University of California, Santa Barbara, CA, 93106-5070, USA

ARTICLE INFO

Article history:

Received 2 August 2020

Accepted 1 September 2020

Available online 30 September 2020

Keywords:

Fe-Al alloy

Compression

High-temperature

Interface

Dislocation

ABSTRACT

Fe-Al compounds possess a combination of high strength and corrosion resistance at high temperatures. However, increasing Al content to make them lighter results in brittleness. Here, we investigate the high-temperature behavior of a novel, lightweight, ultra-fine-layered FeAl/FeAl<sub>2</sub> material. We report a transition from unstable to stable plasticity at 450 °C. Below 450 °C, deformation is dominated by localized shear deformation within the soft FeAl layers, while above 450 °C, it proceeds by co-deformation between FeAl and the brittle FeAl<sub>2</sub> layers. We show that co-deformation is associated with the temperature at which the interface converts from sliding to sourcing dislocations for FeAl<sub>2</sub>.

© 2021 Published by Elsevier Ltd on behalf of The editorial office of Journal of Materials Science & Technology.

## 1. Introduction

Fe-Al alloys are a promising high-temperature, structural material due to their excellent oxidation resistance, low density, and high strength [1–5]. Currently, there is great interest, for instance, in using Fe-Al films as a transition layer in the storage of tritium, an extreme environment application [6–8]. At this moment, however, most studies on Fe-Al alloys focus on the heavier Fe-Al alloys (<50 at.% Al) [9,10], since they are ductile [11]. Yet, considering the increasing demands for lightweight structural materials, the lighter, more oxidation resistant Fe-Al alloys that are richer in Al than those in use today should be explored, enhanced, and employed. One of the main challenges lies in the fact that Al-rich Fe-Al alloys generally have an outstandingly complex, low-symmetry crystal structure (e.g., triclinic) [12–14], unlike the Al-poor alloys, which possess symmetric crystal structures (e.g., body-centered cubic (BCC)). In addition, Al-rich Fe-Al alloys are brittle at room temperature [15,16], bearing hardness and fracture toughness values of ceramics and glasses [17]. This inherent brittleness limits their use in load-bearing applications that require robustness and non-catastrophic failure.

Recently, the strategy of nanolayering, involving combinations of the lightweight brittle, Al-rich phase with the ductile,

Al-poor phase, has been proposed as a way toward overcoming the lightweight/ductility tradeoff afflicting Fe-Al alloys [18–20]. Recently, a eutectoid Fe-Al alloy with alternating FeAl/FeAl<sub>2</sub> layers and a bilayer thicknesses ranging from 5 μm to 260 nm was fabricated [21]. Once their average layer thickness reduced below 1 μm, the ultra-fine layered FeAl/FeAl<sub>2</sub> material showed signs of homogeneous deformation and no crack under room temperature nanoindentation [21]. As candidate materials for high-temperature applications, it is also critical to know whether instabilities would be promoted in this ultra-fine layered FeAl/FeAl<sub>2</sub> material at elevated temperatures. Because the FeAl would soften further, whereas the brittle phase would not, and any special interface-mediated mechanisms, such as interface sliding, may ensue at higher temperatures.

In this work, we examine the high-temperature performance of ultra-fine layered FeAl/FeAl<sub>2</sub> composite. A combination of nano-indentation, micro-pillar compression, and transmission electron microscope (TEM) characterization are performed for a broad temperature range of 150–500 °C. The layered Fe-Al exhibits an abrupt unstable-to-stable transition at 450 °C. Below 450 °C, deformation is unstable, due to slip band formation in the soft FeAl phase, localized slip bands in FeAl<sub>2</sub> and interfacial sliding. Above 450 °C, it shows stable plastic flow and co-deformation between the soft and brittle phases. At the co-deformation temperature 450 °C, the interface becomes a source for dislocations for the brittle FeAl<sub>2</sub> layer, which is the key to thwarting interface sliding, promoting dislocation transmission across the interface.

\* Corresponding author.

E-mail address: [wzhanxjtu@mail.xjtu.edu.cn](mailto:wzhanxjtu@mail.xjtu.edu.cn) (W. Han).

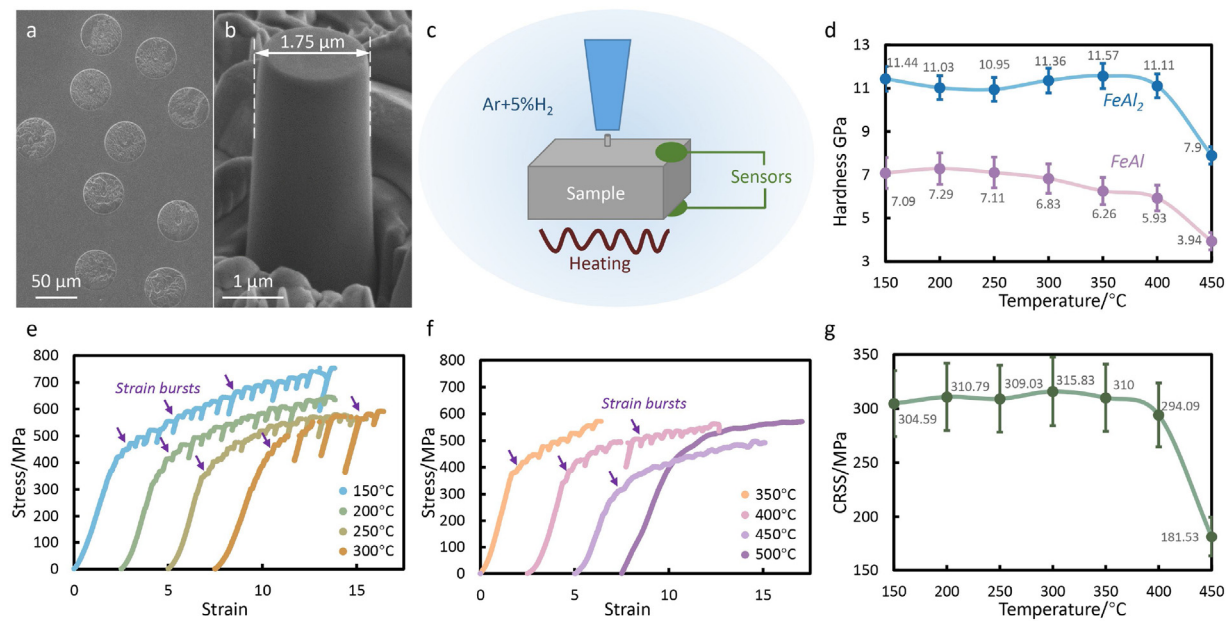


**Fig. 1.** (a) and (b) SEM images of the typical Fe-Al pillar; (c) illustration of the high temperature pillar compression test; (d) variation in hardness for the single-phase FeAl and FeAl<sub>2</sub> phases; (e) and (f) typical compressive stress-strain curves for the layered FeAl/FeAl<sub>2</sub> pillars tested from 150 to 500 °C; (g) evolution of the critical resolved shear stress along (101) plane of FeAl layer.

## 2. Materials and methods

The ultra-fine layered FeAl/FeAl<sub>2</sub> composite with a bilayer thickness of 500 nm was fabricated by arc melting using the methods detailed in Ref [21]. For compression, micro-pillars with a diameter of 1.75 μm and a height of 4.5 μm were prepared from the composite using a focused ion beam (FIB), as shown in Fig. 1(a) and (b). These micro-pillars are milled from different grains so that they would have different orientations with respect to the compression loading direction. Compression was carried out using a high-temperature flat tip under a displacement control mode with a strain rate of  $5 \times 10^{-3} \text{ s}^{-1}$ . Two micro-pillars were tested for each temperature. For reference, hardness tests on the single-phase constituent FeAl and FeAl<sub>2</sub> materials were also performed using a high-temperature Berkovich tip with a load of 5000 μN and holding time of 5 s. Both micro-pillar and hardness tests were performed using a Hysitron TI950 Triboindenter equipped with a high-temperature stage. As illustrated in Fig. 1(c), an Ar+5%H<sub>2</sub>-mixed atmosphere was passed into the chamber to prevent oxidation during testing. Temperature sensors are installed to monitor the testing temperature. The surface morphology of the micro-pillars was examined using a scanning electron microscope (SEM). Deformation microstructures in the micro-pillars were investigated using a JEOL 2100 F TEM by cutting thin foils from the compressed samples.

## 3. Results and discussion

To establish a basis on which to understand the temperature response of the ultrafine composite, we first determined the high temperature hardness of single phase FeAl and FeAl<sub>2</sub> alone. As shown in Fig. 1(d), from 150–400 °C, the hardness of the FeAl phase (the purple line) gradually decreases from 7 to 5.93 GPa, and once the temperature exceeds 400 °C, it drops to 3.94 GPa. In contrast, the hardness of FeAl<sub>2</sub> remains constant, at around 11 GPa, over the range of 150–400 °C and drops sharply to 7.9 GPa when the temperature rises above 400 °C. These tests also reveal that these two materials maintain dissimilar hardness throughout the tempera-

ture range. The FeAl<sub>2</sub> phase is much harder, being 1.57 times the hardness of FeAl.

Fig. 1(e) and (f) displays the series of compressive stress-strain curves of the layered FeAl/FeAl<sub>2</sub> micro-pillars over the temperature range of 150–500 °C. For 150–400 °C, all micro-pillars exhibit frequent strain bursts, as marked in Fig. 1(e), and large stress drops during loading, which are signs of unstable flow. Their yield and, nominally, their flow stresses gradually decrease as temperature increases. At 450 °C, the yield and flow stress are even softer, as would be expected based on similar reductions seen in their hardness with temperature. However, the 450 °C response exhibits no strain bursts and near smooth flow, and signifies a transition to more stable flow. At an even higher temperature, 500 °C, the stress-strain curve is smooth, as shown in Fig. 1(f), and the material is even stronger. These are signs of continuous plastic flow, which is unexpected.

The change to stable flow and concomitant increase in strength at 500 °C suggest a temperature-induced change in deformation mechanism. To identify the underlying mechanisms, TEM analyses are performed on the micro-pillars compressed at 200 °C, when the material is unstable; at 450 °C, the turning point; and at 500 °C. Fig. 2(a) and (b) shows the micro-pillar before and after compression at 200 °C. Oxides on both layers can be seen. These oxides formed due to prolonged heating and are much finer on FeAl<sub>2</sub> layer than on the FeAl layer, due to its higher Al concentration [22,23]. The TEM analysis reveals that the FeAl layers deformed homogeneously (Fig. 2(c)), while the interface shows signs of sliding (Fig. 2(d)) and the FeAl<sub>2</sub> layers signs of localized deformation (Fig. 2(e)). After compression, plastic deformation occurs in the softer FeAl layers, as featured by the extruded metal from the micro-pillar surface and highlighted in Fig. 2(c). The FeAl<sub>2</sub> layers, however, only partially contribute to the deformation, forming some isolated and localized slip bands, as marked in Fig. 2(c). These slip bands are partly responsible for the strain bursts seen in Fig. 1(e). Fig. 2(d) shows evidence of sliding along the  $(1\bar{1}\bar{3})_{\text{FeAl}2}/(101)_{\text{FeAl}}$  FeAl/FeAl<sub>2</sub> interface near the top region of the pillar, another source of the bursts and stress drops. The two white arrows in the right top corner in Fig. 2(d) point to slip steps that have formed as a result of sliding on the top of micro-pillar in

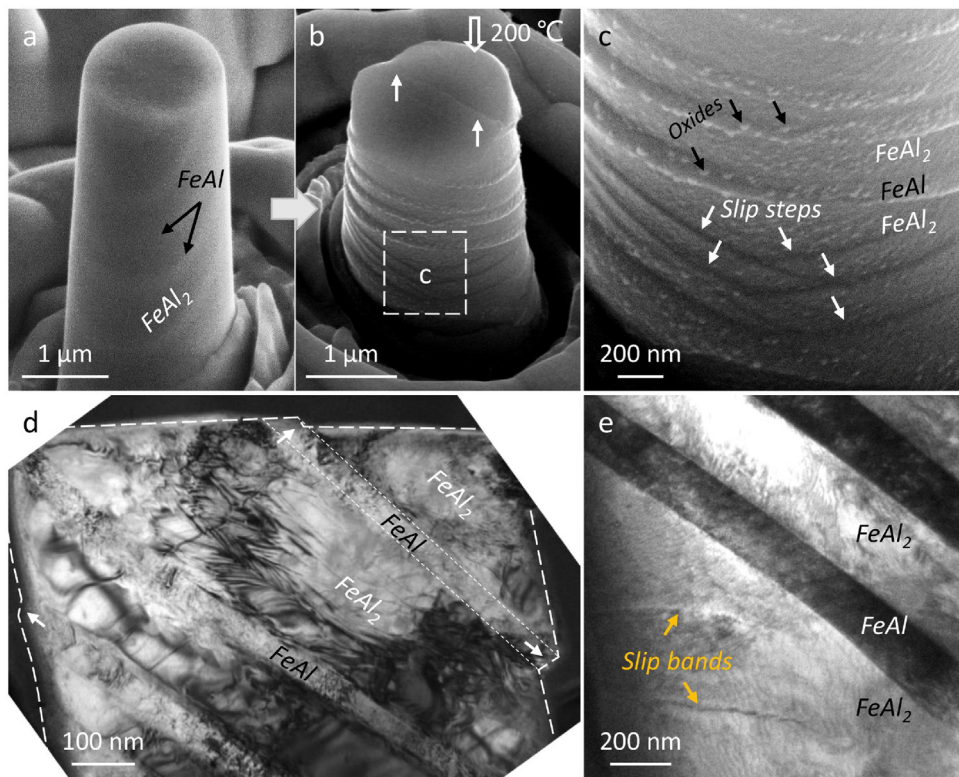


**Fig. 2.** (a) and (b) Typical SEM images of the micro-pillar before and after compression at 200 °C; (c) compression induced extrusion of the FeAl layer and slip steps in the FeAl<sub>2</sub> phase; (d) and (e) TEM images displaying the defect structures after compression.

**Fig. 2(b).** The small steps seen on the left side of the micro-pillar in **Fig. 2(b)** are additional signs of interfacial sliding.

Next, we examine the deformed microstructures in the micro-pillar compressed at 450 °C, the temperature at which a turning point in the compression response is seen. **Fig. 3** presents the images taken from a thin-foil cut in the middle of the compressed micro-pillar. Similar to the micro-pillar compressed at 200 °C, deformation was accommodated primarily by shearing of the FeAl layers and secondly by interfacial sliding. In **Fig. 3(b)**, the right slip step protrudes into the top, while the left slip step is located underneath the FeAl layer, indicating that the entire FeAl layer plastically deformed in micro-pillar compression (**Fig. S1** in Supplementary Materials). Further, the arrows in **Fig. 3(c)** mark evidence of interfacial-sliding-induced steps on both sides of the FeAl layer. Because the (101) interface plane on the FeAl layer side is also a preferred slip plane in FeAl, easy deformation can be accomplished both via slip along the (101) plane in the FeAl layers and along the interface. As shown in **Fig. 1(g)** and Table S1 (in Supplementary Materials), by measuring the angle between the loading axis and the FeAl layers, the critical resolved shear stress (CRSS) for (101) slip can be determined for tests from 200 °C and up to 450 °C. The (101) CRSS is approximately 300 MPa for a broad range of 150–400 °C and drops significantly to 182 MPa at 450 °C.

Regarding the deformation of the FeAl<sub>2</sub> phase, the microscopy analysis still finds it to be inhomogeneous and localized into slip bands at 450 °C. **Fig. 3(c)** shows two pairs of localized bands that have developed in the FeAl<sub>2</sub> layers. Both bands are connected with slip in the FeAl layers, as marked by the yellow dashed lines in **Fig. 3(c)**. A more detailed examination in **Fig. 3(e)** indicates that these bands are a result of slip transmission across the interface. The original interface on the FeAl phase side has protruded due to the concentrated shear from the band and formed a pair of near-90° protrusions on both sides, as marked in **Fig. 3(e)**. The slip bands in the (1̄13) plane in the FeAl<sub>2</sub> layer are directly connected with slip

bands close to the (101) interface plane in the FeAl layer. However, compared to the slip bands formed in FeAl<sub>2</sub> at room temperature [21], the slip bands here are less concentrated and intense, consistent with the observation of less bursts and near smooth flow in **Fig. 1(f)**.

The most remarkable distinction between the response at 450 °C from those at lower temperature pertains to the interaction between the interface and the FeAl<sub>2</sub> layer. **Fig. 3(d)** highlights special dislocation structures that have developed near the FeAl/FeAl<sub>2</sub> interface in FeAl<sub>2</sub> layers at 450 °C, which were not present in the 200 °C sample. These dislocations bow out from the FeAl/FeAl<sub>2</sub> interface, indicating that at 450 °C the interfaces start to act as sources of dislocations for plastic deformation in the FeAl<sub>2</sub> layers. Because the mobility of dislocations in FeAl<sub>2</sub> is still low, these emitted dislocations do not glide further. Evidences of interface dislocation nucleation sites are widely seen in other interfaces in the same deformed micro-pillar, as marked in **Fig. 3(c)**. These findings indicate that at 450 °C, the FeAl<sub>2</sub> phase lies at the threshold of homogeneous plastic deformation.

**Fig. 4** displays the deformed micro-pillar compressed at 500 °C and its internal defects using TEM. Notably, in stark contrast to the micro-pillar compressed at 200 °C and 450 °C, interfacial sliding does not occur, as shown in **Fig. 4(b)** and (c). Although the layers in the pillar have a high inclination angle with respect to the loading axis (**Fig. 4(a)**), which would heighten the applied load to trigger interface sliding, no slip steps can be seen at the intersection of the interface and pillar surface. Even at the bottom, where the material is severely deformed, the interfaces still did not slide, despite the fact that some of the FeAl layers were totally unconstrained (**Fig. 4(c)**). Rather, the layers bend in a coordinated manner, a sign of co-deformation. Evidently at 500 °C, interfacial sliding is shut down, which is consistent with the lack of bursts and stress drops in the response of the micro-pillar. At the point of yielding, the CRSS along the interface for the 500 °C case is about 360 MPa, which is

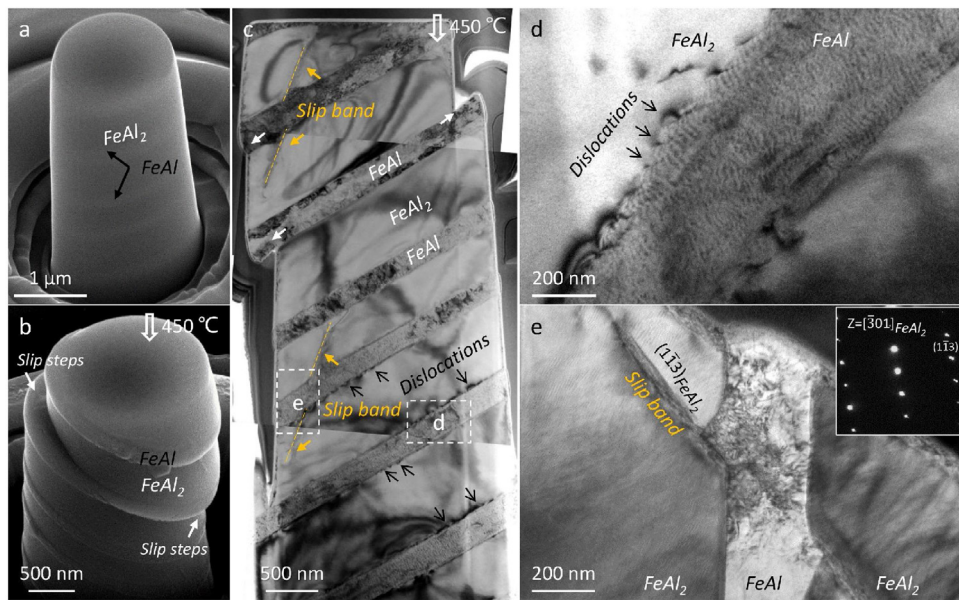


**Fig. 3.** (a) and (b) Typical SEM images showing the pillar before and after compression at 450 °C; (c) TEM image of a thin-foil cut from the deformed pillar; (d) and (e) TEM micrographs showing the defect structures in the pillar after compression.

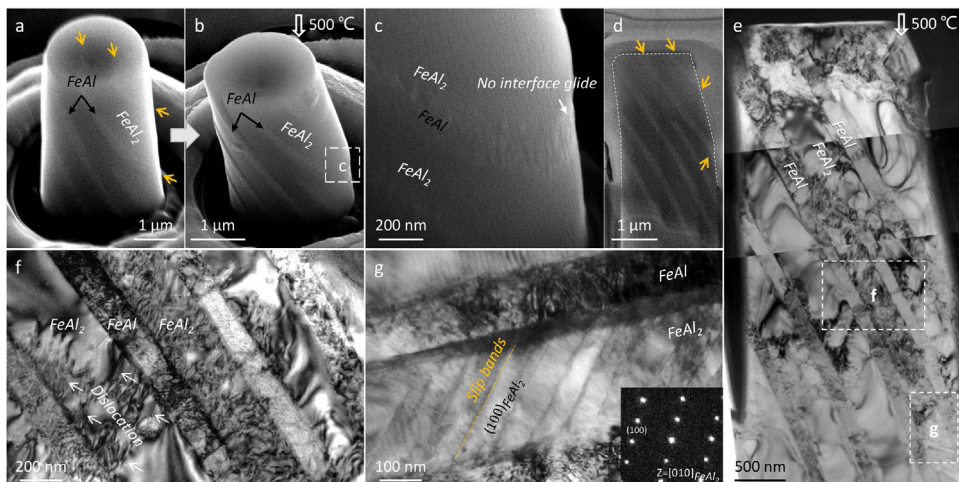


**Fig. 4.** (a) and (b) Typical SEM images of the pillar before and after compression at 500 °C. Although the layers in the micro-pillar have a high inclination angle with respect to the loading axis, the FeAl layers are free to deform, as marked by arrows. (c) Highlight of the surface deformation features. (d) SEM image of the thin-foils cut from deformed pillar. The yellow arrows mark the unconstrained layers. (e)–(g) TEM images showing defect structures in the compressed pillar.

much larger than the CRSS of interface sliding at lower temperature shown in Fig. 1(g). This comparison indicates that the interfacial sliding shut down at 500 °C makes the FeAl/FeAl<sub>2</sub> micro-pillar much stronger.

To understand the cause for stable flow and high strength, we cut a thin-foil from the deformed pillar at 500 °C (Fig. 4(d)) and performed detailed TEM characterization. The analysis reveals that the FeAl<sub>2</sub> phase remarkably co-deforms plastically and compatibly with the FeAl phase. As shown in Fig. 4(e), a large number of dislocations are observed in both the FeAl and FeAl<sub>2</sub> layers, as marked by white arrows in Fig. 4(f). These dislocations were emitted from the interface and into the FeAl<sub>2</sub> phase. At the root of the pillar (Fig. 4(e)), where the pillar appears severely deformed, a set of parallel (100) slip bands in the FeAl<sub>2</sub> layer has developed (Fig. 4(g)). Thus, we find that the interface enables the FeAl<sub>2</sub> layers to deform homogeneously, like their adjoining FeAl layers, by acting as a source for dislocations for the FeAl<sub>2</sub> layers and supporting frequent FeAl-FeAl<sub>2</sub> slip transmission across the interface.

Both high-temperature nanoindentation and micro-pillar tests indicate that the hardness of the ductile single-phase FeAl continues to decrease with increasing temperature, a general trend that has been reported previously [24]. The FeAl phase has a B2 ordered structure and it is well known that its primary slip mode is {110} <111>, similar to the preferred slip mode in pure BCC metals. Studies have reported that when the temperature exceeds ~300–350 °C in FeAl, slip on the {110} <100> systems [25] or on both the {110}<100> and {110}<111> systems have been observed [25]. Here, in the ultra-fine layered composites, the gradual softening in the FeAl phase with temperature is related to the activation of the {110}<100> slip systems in addition to the {110}<111> slip systems.

The analyses of this study reveal that the role of the interface in the layered FeAl/FeAl<sub>2</sub> changes over the temperature range studied here. At 150–200 °C, interfacial sliding acts as a deformation mechanism. The interface plane (101) on the FeAl side is known as an easy glide plane in B2 FeAl (Fig. 2) and similar responses were

seen at room temperature [21]. Otherwise, the individual phases behave much like their bulk counterparts. The FeAl layers deform homogeneously, and dislocations glide easily within the FeAl layer on the  $(101)<11\bar{1}-1>$  slip systems. The  $\text{FeAl}_2$  layers deform unstably via the formation of a small fraction of highly concentrated shear bands. Taken together, slip in FeAl layers, unstable interfacial sliding, and shear bands in  $\text{FeAl}_2$  layers result in serrated flow in Fig. 1(e). As the temperature increases to 450 °C, a turning point in the response, an additional slip mode, the  $\{110\}<100>$  mode, is activated in the FeAl layers. This deformation is accompanied by even more deformation accommodation by interface sliding, as shown by a sudden drop in the measured CRSS and larger slip steps on the deformed pillar. However, as the main change, evidence of incipient dislocation nucleation from the interface into the  $\text{FeAl}_2$  side is revealed, although it is apparent that dislocation mobility is still low. With further increase in temperature up to 500 °C, dislocations nucleate from the interface and dislocation mobility in  $\text{FeAl}_2$  phase is enhanced, as manifested by the high density of dislocations in Fig. 4(e). Slip transmission across the interface into the FeAl leads to co-deformation of both FeAl and  $\text{FeAl}_2$  layers. Thus, above 450 °C, rather than stable slip only in the FeAl layers, the interfaces become sources of dislocations in both FeAl and  $\text{FeAl}_2$  layers, enabling co-deformation and making the micro-pillar stronger.

#### 4. Conclusion

In summary, we performed micro-pillar tests in the temperature range of 150–500 °C in a lightweight, ultra-fine layered FeAl/ $\text{FeAl}_2$ . An unstable-to-stable transition is observed at 450 °C, which manifests as a change in material response from serrated flow to homogeneous flow. This behavior is associated with a transition from plastic deformation primarily in the soft FeAl phase, widely separated, localized slip bands in the  $\text{FeAl}_2$  phase, and interface sliding to interfacial-emission of dislocations into the brittle  $\text{FeAl}_2$ , enabling co-deformation between FeAl and  $\text{FeAl}_2$  layers and higher strength in micro-pillar.

#### Declaration of Competing Interest

The authors declare no conflict of interest.

#### Acknowledgements

This work was financially supported by the National Natural Science Foundation of China (Nos. 51922082, 51971170 and

51942104), the National Key Research and Development Program of China (No. 2017YFB0702301), the 111 Project of China (No. BP2018008), and the Innovation Project of Shaanxi Province (No. 2017KTPT-12).

#### Appendix A. Supplementary data

Supplementary material related to this article can be found, in the online version, at doi:<https://doi.org/10.1016/j.jmst.2020.09.018>.

#### References

- [1] N.S. Stoloff, Mater. Sci. Eng. A 258 (1998) 1–14.
- [2] J. Cebulski, D. Pasek, in: M. Aliofkhazraei (Ed.), *FeAl Intermetallic Alloy: Its Heat-Resistant and Practical Application, Intermetallic Compounds-Formation and Applications*, IntechOpen, Norderstedt, 2018.
- [3] K. Bobzin, M. Öte, S. Wiesner, L. Gerd, JOP Conf. Ser. Mater. Sci. Eng. 373 (2018), 012013.
- [4] M. Zamanzade, A. Barnoush, C. Motz, Crystals 6 (2016) 10.
- [5] M. Palm, F. Stein, G. Dehm, Annu. Rev. Mater. Res. 49 (2019) 297–326.
- [6] D.G. Morris, M.A. Muñoz-Morris, Adv. Eng. Mater. 13 (2011) 43–47.
- [7] G.K. Zhang, X.L. Wang, F.L. Yang, Y. Shi, J.F. Song, X.C. Lai, Int. J. Hydrogen Energy 38 (2013) 7550–7560.
- [8] F.L. Yang, X. Xiang, G.D. Lu, G.K. Zhang, T. Tang, Y. Shi, X.L. Wang, J. Nucl. Mater. 478 (2016) 144–148.
- [9] C.T. Liu, E.P. George, P.J. Maziasz, J.H. Schneibel, Mater. Sci. Eng. A 258 (1998) 84–98.
- [10] S. Kobayashi, T. Yakou, Mater. Sci. Eng. A 338 (2002) 44–53.
- [11] O. Ikeda, R. Kainuma, I. Ohnuma, K. Fukamichi, K. Ishida, Intermetallics 9 (2001) 755–761.
- [12] F. Stein, S.C. Vogel, M. Eumann, M. Palm, Intermetallics 18 (2010) 150–156.
- [13] I. Chumak, K.W. Richter, H. Ehrenberg, Acta Crystallogr. Sect. C Cryst. Struct. Commun. 66 (2010) 87–88.
- [14] X.L. Li, A. Schmitt, M. Heilmaier, F. Stein, J. Phase Equilib. Diffus. 37 (2016) 162–163.
- [15] C.H. Zhang, S. Huang, J. Shen, N.X. Chen, Intermetallics 52 (2014) 86–91.
- [16] D. Chanbi, L.A. Amara, E. Ogam, S.E. Amara, Z. Fellah, Materials 12 (2019) 433.
- [17] P. Matysik, S. Józwik, T. Czuiko, Materials 8 (2015) 914–931.
- [18] A. Donohue, F. Spaepen, R.G. Hoagland, A. Misra, Appl. Phys. Lett. 91 (2007), 241905.
- [19] J.L. Wang, A. Misra, Curr. Opin. Solid State Mater. Sci. 18 (2014) 19–28.
- [20] N. Li, H.M. Wang, A. Misra, J. Wang, Sci. Rep. 4 (2015) 6633.
- [21] L.L. Li, Y.Q. Su, I.J. Beyerlein, W.Z. Han, Sci. Adv. 6 (2020) eabb6658.
- [22] Z.Y. Liu, G. Wei, F.H. Wang, Scr. Mater. 39 (1998) 1497–1502.
- [23] A. Scherf, D. Janda, M.B. Yazdi, X.L. Li, F. Stein, M. Heilmaier, Oxid. Met. 83 (2015) 559–574.
- [24] M. Windmann, A. Röttger, I. Hahn, W. Theisen, Surf. Coat. Technol. 321 (2017) 321–327.
- [25] M.G. Mendiratta, H.M. Kim, H.A. Lipsitt, Metall. Mater. Trans. A 15 (1984) 395–399.